# Effects of free-stream turbulence intensity on transition within a laminar separation bubble

**Mark S. Istvan and Serhiy Yarusevych***

Department of Mechanical and Mechatronics Engineering
University of Waterloo
200 University Ave. W, Waterloo, ON, N2L3G1, Canada
*syarus@uwaterloo.ca

## ABSTRACT

The laminar separation bubble formed over the suction side of a NACA 0018 airfoil was studied experimentally for increasing levels of free-stream turbulence intensity. Experiments were performed in a wind tunnel facility at a chord Reynolds number of 80 000 and an angle of attack of 4 degrees. The spatio-temporal flow development was characterized by means of time-resolved Particle Image Velocimetry. The results show that the height and streamwise extent of the separation bubble are reduced as the level of turbulence intensity is increased. The decrease in separation bubble length is the result of downstream and upstream shifts in the locations of mean separation and reattachment, respectively, with the later caused by an upstream shift in the location of mean transition. Velocity fluctuations in the shear layer reach significant magnitudes earlier upstream as the level of turbulence intensity is increased, leading to the upstream shift in mean transition. At the highest level of turbulence intensity investigated, significant changes occur in the flow topology and dynamics, suggesting an alteration of the transition process. Maximum spatial amplification rates of disturbances are shown to decrease as the bubble size decreases, indicating that the upstream shift in mean transition is attributed to the increase in the initial amplitude of disturbances upstream of the separation bubble. Spectra of the wall-normal velocity fluctuations show that, as the bubble size is reduced, the central frequency of disturbances remains approximately constant, but that the detectable band of unstable frequencies broadens as a result of the broader range of disturbances present in the free-stream.

## INTRODUCTION

Laminar separation bubbles (LSBs) have been an area of active research for several decades (Gaster, 1967; Mueller, 1985; Watmuff, 1999; Kurelek *et al.*, 2016). LSBs typically form over airfoils operating at chord Reynolds numbers ($Re_c$) below approximately 500 000 (Carmichael, 1981), which is a range relevant to a number of applications including small to medium sized wind turbines and unmanned aerial vehicles. Their presence can increase drag, thereby reducing airfoil performance as compared to that at higher chord Reynolds numbers (Lissaman, 1983). Understanding the flow development within LSBs is of interest to engineers for improving airfoil performance and to better implement flow control systems.

LSBs form as a consequence of laminar boundary layer separation. Downstream of the suction peak, the flow faces an adverse pressure gradient which, if large enough, will cause the flow to separate. The resulting separated shear layer then undergoes transition to turbulence, and the enhanced momentum exchange can lead to mean flow reattachment if transition in the separated shear layer occurs shortly after separation. When reattachment does occur, the resulting time-averaged recirculating flow region is referred to as the laminar separation bubble (Tani, 1964; Gaster, 1967). The transition process in the separated shear layer has become the emphasis of research more recently due to its importance in the overall flow development, and the emergence of more powerful measurement techniques (Watmuff, 1999; Burgmann & Schröder, 2008; Boutilier & Yarusevych, 2012*b*). In low-disturbance environments, the transition process in the separated shear layer begins with the amplification of small amplitude disturbances originating upstream as a result of the receptivity process (Saric *et al.*, 2002). The initial amplification of these disturbances can be well-modelled using Linear Stability Theory (Marxen *et al.*, 2003; Boutilier & Yarusevych, 2012*b*). Later in the transition process non-linear interactions begin to occur and the separated shear layer rolls up, leading to the periodic shedding of spanwise coherent structures which dominate flow development in the aft portion of the bubble (Yarusevych *et al.*, 2009; Kurelek *et al.*, 2016).

The transition process in the separated shear layer is sensitive to the initial amplitudes and frequency content of disturbances and, thus, the effects of flow conditions within research facilities on the flow over airfoils at low Reynolds numbers has been considered in several studies. It has been shown that free-stream turbulence intensity can have a significant influence on airfoil performance (Mueller *et al.*, 1983; Cao *et al.*, 2011) as well as on LSB characteristics (O'Meara & Mueller, 1987; Ol *et al.*, 2005; Olson *et al.*, 2013; Istvan *et al.*, 2016). Ol *et al.* (2005) showed that, for nominally identical experimental settings in different facilities, the locations of mean separation, transition, and reattachment over an SD 7003 airfoil can vary by as much as 10% of the chord length. These differences were attributed, in part, to differences in the free-stream turbulence intensities of about 0.1% between the facilities. By using a turbulence generating grid to increase the turbulence intensity from 0.3% to 0.9% in their facility, Olson *et al.* (2013) showed that the locations of mean separation and reattachment over the same SD 7003 airfoil shifted downstream and upstream by 3% and 12% of the airfoil chord length, respectively. The results of Istvan *et al.* (2016) showed that for increasing levels of turbulence intensity, the length of the LSB formed over a NACA 0018 airfoil was reduced as a result of an upstream shift in the locations of mean transition and reattachment. Using fluctuating surface pressure measurements, the authors showed that the onset of significant shear layer disturbance amplification occurred further upstream for increasing levels of turbulence intensity, resulting in the upstream shifts of mean transition and reattachment. Previous investigations have focused on airfoil performance as well as characterizing the mean topology of separation bubbles for increasing levels of free-stream turbulence intensity, while the accompanying changes in the flow dynamics within LSBs remain unclear.

The purpose of this investigation is to examine experimentally the effects of free-stream turbulence intensity on the transition process within a laminar separation bubble formed over a NACA 0018 airfoil at a chord Reynolds number of 80 000 and an angle of attack of 4°. The spatio-temporal flow development of the separation bubble is characterized using planar, two-component Particle Image Velocimetry in order to shed light on the effect of turbulence

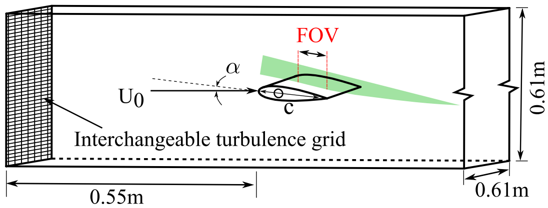


Figure 1: Experimental arrangement.

intensity on LSB dynamics.

## EXPERIMENTAL SET-UP

All experiments were performed in the recirculating wind tunnel at the University of Waterloo, featuring a test section that is 0.61 m wide by 0.61 m high, and 2.4 m long. The flow is conditioned by aluminum honeycomb and a set of five turbulence reducing screens upstream of a 9 : 1 contraction leading into the test section. Experiments were performed using an aluminum NACA 0018 airfoil, having a chord length and span of 0.2 m and 0.6 m, respectively. The model was mounted horizontally in the test section, as depicted in Fig. 1. In order to prevent tonal noise emission from the trailing edge of the airfoil, which has been shown to develop a feedback loop with the suction side LSB (Pröbsting & Yarusevych, 2015), a 10 mm wide strip of randomly distributed roughness elements was placed on the pressure side of the airfoil at $x/c \approx 0.3$ to trip the boundary layer and prevent separation.

The level of free-stream turbulence intensity (*Tu*) was increased by inserting turbulence generating grids just upstream of the test section inlet, as shown in Fig. 1. The free-stream characteristics were assessed using hotwire anemometry. A normal hotwire probe, operated with a Dantec Streamline Constant Temperature Anemometer unit, was placed in the empty test section at the location corresponding to the midspan of the leading edge of the airfoil. The hotwire was calibrated in-situ against a Pitot-static tube placed approximately 3 cm below it. The analogue signal was sampled at 100 kHz, for a total of $2^{23}$ samples, and low-pass filtered at 50 kHz. Turbulence intensities were computed as the root-mean-square of the velocity fluctuations low-pass filtered at 25 kHz. Correlation lengths ($\Lambda$) in the free-stream were computed by integrating an exponential fit to the autocorrelation function of the velocity signal and then, assuming Taylor's frozen turbulence hypothesis, multiplying the obtained value by the mean free-stream velocity. A summary of the investigated flow conditions is provided in Table 1, where case i) corresponds to the baseline conditions in the test section.

Spectra of the free-stream velocity fluctuations were computed using Welch's method (Welch, 1967). Here, the entire length of the velocity signal was divided into windows of $2^{17}$ samples with 50% overlap. Spectra were computed for each window and averaged to

Table 1: Investigated free-stream conditions.

| | Case | | | |
|---|---|---|---|---|
| | i) | ii) | iii) | iv) |
| *Tu* [%] | 0.11 | 0.22 | 0.50 | 1.92 |
| $\Lambda$ [mm] | 64.54 | 4.13 | 4.14 | 6.54 |

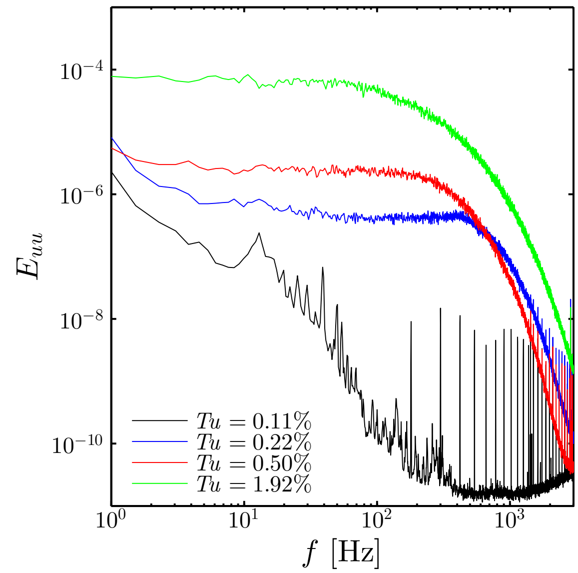


Figure 2: Spectra of free-stream velocity fluctuations.

yield a frequency resolution of 0.8 Hz, and are shown in Fig. 2. The results show that there are no dominant frequencies introduced into the flow by the turbulence generating grids. At the baseline level of *Tu*, there is a notable spectral peak at 15 Hz which is associated with the tunnel's fan blade-passage frequency, and is also notable at higher *Tu* levels. However, this frequency is about an order of magnitude lower than the lowest flow frequency of interest.

Two-component Particle Image Velocimetry (PIV) was employed in two side-view configurations: 1) a two camera, time-resolved system was used to characterize the spatio-temporal flow development, and 2) a single higher-resolution camera was employed. In the first configuration, two $1024 \times 1024$ px Photron SA4 cameras were used to simultaneously image the entire separation bubble. The cameras were equipped with 200 mm Nikon lenses and the magnification factor was adjusted for each level of *Tu* investigated in order to maximize the spatial resolution. For the second configuration, a single $1600 \times 1200$ px LaVision Pro-X camera was used, equipped with a 200 mm Nikon lens. The camera was placed on a three axis traverse and, for all levels of *Tu* investigated, five $18 \times 13$ mm fields-of-view (FOV) were imaged by traversing the

Table 2: Summary of important PIV parameters.

| | Configuration | |
|---|---|---|
| | 1) | 2) |
| Samples | 5000 | 1000 |
| Sampling rate | 3 kHz | 15 Hz |
| Frame separation | 60 to 80 $\mu$s | 23 $\mu$s |
| Sensor size | $1024 \times 1024$ px | $1600 \times 1200$ px |
| Mag. factor | 0.49 to 0.66 | 0.66 |
| Total FOV | $0.3\ell \times 0.06\ell$ | $0.4\ell \times 0.05\ell$ |
| Vector pitch | 0.12 to 0.17 mm | 0.05 mm |

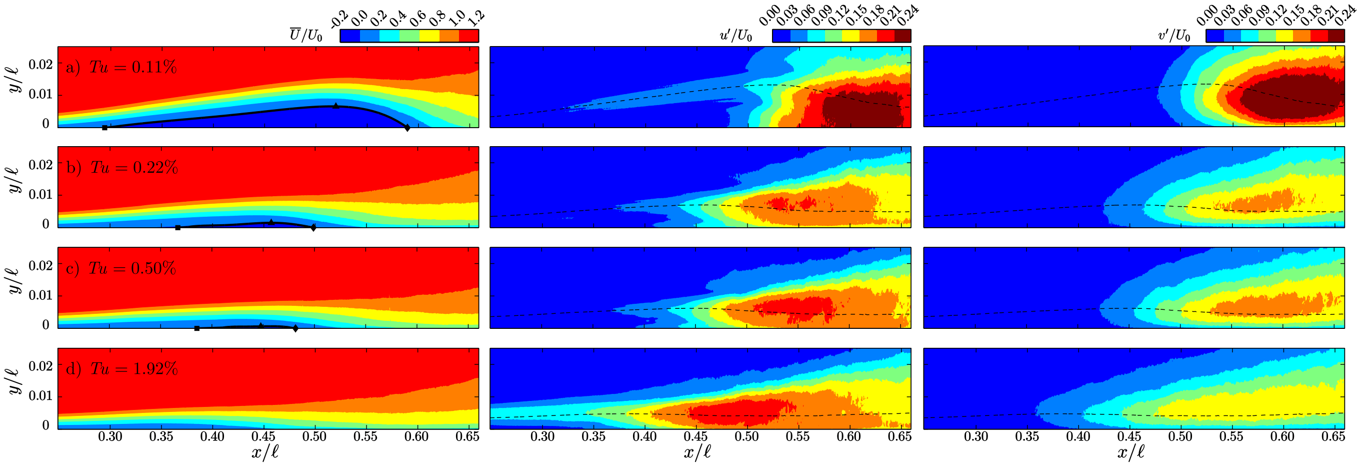


Figure 3: Contours of mean streamwise velocity (left), root-mean-square of streamwise velocity fluctuations (centre), and root-mean-square of wall-normal velocity fluctuations (right). Solid black lines trace the dividing streamline while dashed black lines show the boundary layer displacement thickness. Square, triangle, and diamond markers represent the locations of mean separation, maximum bubble height, and reattachment, respectively.

camera in the streamwise direction, and were subsequently stitched together. For both configurations, the flow was seeded with a water-glycol based fog (mean particle diameter of 4 $\mu$m). The flow was illuminated in the first configuration using a Photonics DM20-527 high-repetition rate, Nd:YLF laser. For the second configuration, an EverGreen 70 Nd:YAG laser was used. The laser beam in both cases was conditioned into a sheet approximately 1 mm thick using the same set of optics. The experimental arrangement is sketched in Fig. 1. Particle images were acquired in double-frame mode at 3000 Hz and 15 Hz for the time-resolved and non-time-resolved configurations, respectively. For both configurations, the laser and cameras were synchronized using a LaVision timing unit controlled through LaVision's DaVis 8 software. Images were processed in DaVis 8 using a multi-pass cross-correlation algorithm with window deformation and a final window size of $16 \times 16$ px, with 75% overlap. Velocity fields from the PIV results were stitched together and transformed into surface-attached coordinates with the origin located at the leading edge of the airfoil. A summary of the important PIV parameters for the two configurations is provided in Table 2.

## RESULTS

All results presented here pertain to a chord Reynolds number of 80000 and an angle of attack of 4°.

Contours of mean streamwise velocity, acquired using the low-speed PIV system are presented in the left column of Fig. 3. At the baseline level of *Tu*, the results show the topology representative of a laminar separation bubble (LSB), characterized by a distinct, elongated, time-averaged reverse flow region adjacent to the airfoil surface. The thick black line traces the contour of zero mean velocity (*i.e.* the dividing streamline) and outlines the LSB. The intersections of this line with the surface of the airfoil correspond to the locations of mean separation ($x_S$) and reattachment ($x_R$). The location of the maximum bubble height ($x_h$) is also shown along the dividing streamline. The location of maximum bubble height was determined as the location of the peak value of the boundary displacement thickness (presented in Fig. 5), and is indicative of the location of mean transition (Boutilier & Yarusevych, 2012*b*). As the level of *Tu* is increased, the extent of the separated region is significantly reduced. The results show that the separation bubble length decreases as a result of a downstream shift in the location of mean separation, as well as an upstream shift in the location of mean reattachment, consistent with the results of Olson *et al.* (2013). The location of maximum bubble height also shifts upstream with increasing *Tu*, indicating that the location of mean transition shifts upstream with increasing *Tu*. The streamwise locations of mean separation, maximum bubble height, and mean reattachment, as well as the separation bubble length ($\ell_b = x_R - x_S$) are summarized in Fig. 4. The results show that by doubling the *Tu* level from 0.11% to 0.22%, the separation bubble length is approximately halved. For the further increase in *Tu* to 0.50%, which is approximately double the turbulence intensity of the 0.22% case, the changes in the locations of mean separation and reattachment are checked. This result is an indication that the effects of increasing *Tu* on the separation bubble may saturate at some upper limit.

At the highest *Tu* level investigated, a time-averaged reverse flow region indicative of a separation bubble could not be identified (Fig. 3d). However, the shape of the mean velocity contours is consistent with those seen at the lower levels of *Tu*, which suggests that a separation bubble is present, but the reverse flow region is simply not resolved by the measurements. To quantitatively support this assertion, boundary layer displacement thicknesses are presented in Fig. 5. At the baseline level of *Tu*, the displacement thickness increases with streamwise distance until it reaches a peak, indicative of transition (Boutilier & Yarusevych, 2012*b*). The value of $\delta^*$ then decreases downstream of this point as the flow reattaches and a tur-

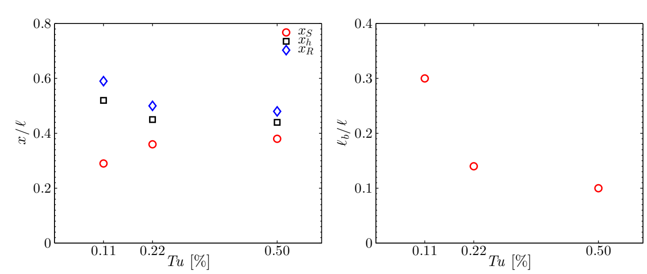


(a) (b)

Figure 4: a) locations of mean separation, maximum bubble height, and reattachment, and b) separation bubble length.

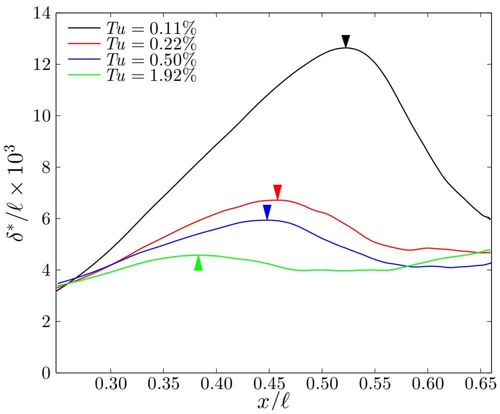


Figure 5: Boundary layer displacement thickness. Arrows indicate the locations of the maxima.

bulent boundary layer develops. Similar behaviour is noted for all elevated levels of *Tu*. In addition, the peak in $\delta^*$ shifts upstream with all increases in *Tu*, consistent with the movement of the separation bubble seen in Fig. 4a. The fact that the results pertaining to the highest *Tu* level investigated feature a distinct peak in the displacement thickness would support the earlier assertion that a very small separation bubble is present at this condition.

To investigate changes in transition leading to the observed changes in mean bubble topology, contours of the root-mean-square (RMS) of velocity fluctuations in the streamwise and wall-normal directions are presented in Fig. 3. At the baseline level of *Tu*, three distinct peaks are observed in the contours of $u'$ around $x/\ell = 0.50$, consistent with previous results of transition over an airfoil in a low-disturbance environment (*e.g.* Boutilier & Yarusevych, 2012*b*). The wall-normal location of the middle peak aligns closely with the displacement thickness, shown by the dashed black line, and is associated with velocity fluctuations in the separated shear layer. When the level of *Tu* is increased to 0.22% and then to 0.5%, the same triple peak structure can still be identified. In contrast, $v'$ contours feature a single dominant peak closely aligned with the displacement thickness. The increase in *Tu* also leads to more significant velocity fluctuations to be attained earlier upstream, which is more clearly seen in $v'$ contours, confirming the upstream shift in mean transition location deduced from Fig. 5. It should be noted that elevated $u'$ values observed in the fore portion of the separation bubble for the baseline case are likely attributed to bubble flapping, which produces notable fluctuations in the local streamwise velocity due to the vertical movement of the separated shear layer. Similar to the previously discussed trends, the effect of increasing *Tu* level is checked for $Tu = 0.5\%$. However, increasing the turbulence intensity to 1.92% produces significant changes in the rms of the streamwise velocity fluctuations, with notable fluctuations in $u'$ seen upstream of the separation bubble. This indicates that the upstream boundary layer is transitional upstream of the likely separation bubble location. At this *Tu* level, increases in the vertical velocity fluctuations occur further downstream which is consistent with the formation and shedding of shear layer vortices observed in the time resolved results for this and lower levels of *Tu*.

The spatial distribution of streamwise velocity fluctuations observed for $Tu = 1.92\%$ in the present study is similar to that reported by McAuliffe & Yaras (2010) (see Fig. 11 in their work) who simulated the effects of free-stream turbulence intensity by increasing the level of incoming pertubations in their numerical modeling of an LSB on a flat plate subjected to an adverse pressure gradient. McAuliffe & Yaras (2010) attributed the large magnitudes of $u'$ upstream of separation to streamwise oriented streaks forming within the boundary layer, which contributed little to $v'$. These types of streaks have also been identified by other investigators (Matsubara & Alfredsson, 2001; Zaki, 2013) in boundary layers subject to high levels of *Tu*. In the present investigation, evidence of these streaks was seen in top-view PIV data and further indicates that the transition process is likely altered at this high *Tu* level compared to that at lower free-stream turbulence intensities.

To provide added insight into the amplification of velocity fluctuations in the separated shear layer, Fig. 6 presents the variation of $u'$ and $v'$ along the displacement thickness. For a given component of velocity, the results show nearly exponential growth of the velocity fluctuations within the separation bubble. Near the location of mean reattachment, fluctuation growth saturates and the velocity fluctuations reach maximum amplitudes, consistent with the results of previous investigations of transition within an LSB (Gerakopulos & Yarusevych, 2012; Boutilier & Yarusevych, 2012*b*). While the maximum amplitude of streamwise fluctuations is comparable for different *Tu* levels, notably higher maximum vertical velocities are observed for the baseline case. A similar trend was observed by Yarusevych & Kotsonis (2017*b*), and is linked to the changes in the height of the separation bubble, with closer proximity of the wall dampening vertical fluctuations produced by the shear layer vortices. The spatial amplification of the disturbances in the separated shear layer can be quantified using an amplification factor (Boutilier & Yarusevych, 2012*a*), defined here as $\sigma = \ln(\Delta v'/U_0)/(\Delta x/\ell)$. The points used to calculate the maximum spatial amplification factors ($\sigma_{max}$) are indicated in Fig. 6b for each *Tu* level. The obtained values are summarized in Table 3 and show that, as the level of *Tu* is increased, the maximum spatial amplification rate of shear layer perturbations decreases. This decrease in the spatial amplification factor is attributed to the reduction in the size of the separation bubble. Using plasma actuators, Yarusevych & Kotsonis (2017*a*) noted a decrease in the maximum disturbance growth rate of approximately 40% when the bubble length was approximately halved. Here, when the mean bubble length is reduced by about 50% for $Tu = 0.5\%$, the maximum amplification factor decreases by approximately 30%. The reduction in the amplification rates of the disturbances at higher *Tu* implies that the upstream shift in the location of mean transition with increasing *Tu* is largely the result of increased initial amplitudes of disturbances.

To characterize the frequency content of the velocity fluctuations within the separated shear layer, spectra of the wall-normal velocity fluctuations measured by the time-resolved PIV system are considered. The spectra at several streamwise locations along the

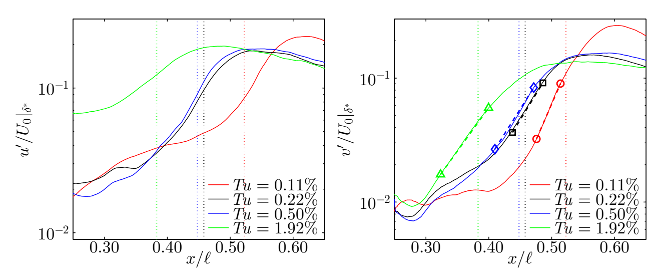


(a) (b)

Figure 6: Variation of a) $u'$ and b) $v'$ along the boundary layer displacement thickness. Dotted lines correspond to the locations of mean transition, while in b) the dashed lines connecting the markers identify the regions for which amplification factors are computed (Table 3).

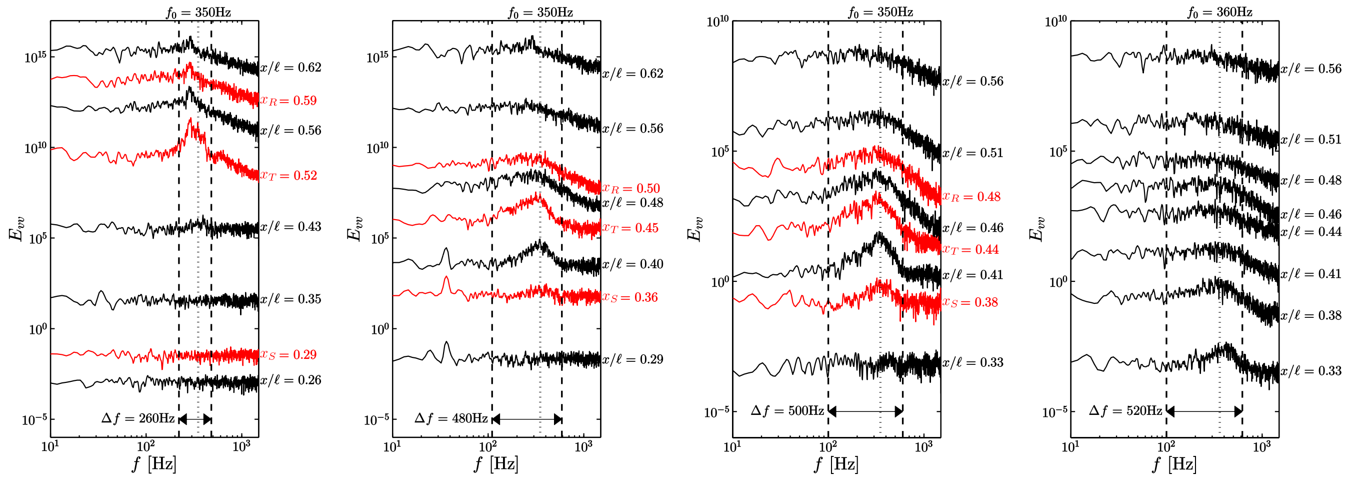


(a) $Tu = 0.11\%$ (b) $Tu = 0.22\%$ (c) $Tu = 0.50\%$ (d) $Tu = 1.92\%$

Figure 7: Spectra of wall-normal velocity fluctuations sampled at the height of the displacement thickness. For clarity, all spectra have been normalized and stepped by an order of magnitude proportional to the streamwise location of the measurement station. Spectra at the locations of mean separation, transition, and reattachment are coloured red.

displacement thickness are shown in Fig. 7. For all the levels of *Tu* investigated, the spectra show the same general behaviour. As the flow develops downstream of mean separation, velocity fluctuations within a band of unstable frequencies ($\Delta f$) centred on some central frequency ($f_0$) are amplified. Around the location of mean transition, the energy content associated with the unstable frequency band begins to spread across a wider range of frequencies. Downstream of mean reattachment, the spectra resemble those typical of a turbulent boundary layer. The results show that, as the level of *Tu* is increased, the width of the amplified disturbance band increases, while the central frequency remains approximately constant. The increase in the width of the unstable frequency band is attributed to the higher energy content of the background disturbances across a wider range of frequencies (Fig. 2). Once amplified in the separated shear layer, the associated velocity fluctuations become measurable above the noise level earlier upstream due to the higher initial amplitude of perturbations.

## CONCLUSIONS

The effects of free-stream turbulence intensity on the separation bubble formed over the suction side of a NACA 0018 airfoil were investigated experimentally for a chord Reynolds number of 80 000 and an angle of attack of 4°. The results show that the size of the separation bubble is reduced as the level of turbulence intensity is increased. The decrease in separation bubble length is attributed to a downstream shift in the location of mean separation and an upstream shift in the location of mean reattachment, the later being the result of an upstream shift in the location of mean transition.

At higher *Tu* levels, velocity fluctuations in the separated shear layer reach significant amplitudes earlier upstream, leading to earlier transition and reattachment. At the highest level of *Tu* investigated, streamwise velocity fluctuations contain significant fluctuations upstream of the likely location of the separation bubble, which indicates an alteration to the transition process linked to the advanced development of perturbations in the boundary layer upstream of separation. Maximum spatial amplification rates are shown to decrease with decreasing separation bubble size, indicating that the increase in initial disturbance amplitude upstream of the separation bubble is the main factor responsible for the upstream shift in mean transition and, thus, reattachment.

Spectra of wall-normal velocity fluctuations show that, as the level of free-stream turbulence is increased, the fundamental frequency of the bubble is not altered significantly but the band of detectable amplified frequencies broadens. The broadening of the unstable frequency band is the consequence of more significant energy content within a broader range of frequencies in the free-stream disturbances, which produces measurable velocity fluctuations over a broader frequency range earlier upstream.

Table 3: Summary of shear layer velocity fluctuation characteristics.

| | *Tu* [%] | | | |
|---|---|---|---|---|
| | 0.11 | 0.22 | 0.50 | 1.92 |
| $\sigma_{max}$ | 134.9 | 95.3 | 92.6 | 80.8 |
| $f_0$ [Hz] | 350 | 350 | 350 | 360 |
| $\Delta f$ [Hz] | 260 | 480 | 500 | 520 |

## ACKNOWLEDGEMENTS

The authors gratefully acknowledge the Natural Sciences and Engineering Research Council of Canada (NSERC) and Bombardier Aerospace for funding this work.

## REFERENCES

Boutilier, M. S. & Yarusevych, S. 2012*a* Parametric study of separation and transition characteristics over an airfoil at low Reynolds numbers. *Exp. Fluids* **52** (6), 1491–1506.

Boutilier, M. S. & Yarusevych, S. 2012*b* Separated shear layer transition over an airfoil at a low Reynolds number. *Phys. Fluids* **24** (8), 084105.

Burgmann, S. & Schröder, W. 2008 Investigation of the vortex induced unsteadiness of a separation bubble via time-resolved and scanning PIV measurements. *Exp. Fluids* **45** (4), 675–691.

Cao, N., Ting, D. S.-K. & Carriveau, R. 2011 The Performance of a High-lift Airfoil in Turbulent Wind. *Wind Eng.* **35** (2), 179–196.

Carmichael, B. H. 1981 Low Reynolds number airfoil survey, volume 1. *Tech. Rep.*. NASA.

Gaster, M. 1967 The Structure and Behaviour of Laminar Separation Bubbles. *Aeronaut. Res. Counc.* **RM 3595**.

Gerakopulos, R. & Yarusevych, S. 2012 Novel Time-Resolved Pressure Measurements on an Airfoil at a Low Reynolds Number. *AIAA J.* **50** (5), 1189–1200.

Istvan, M. S., Kurelek, J. W. & Yarusevych, S. 2016 Effects of free-stream turbulence intensity on laminar separation bubbles. In *46th AIAA Fluid Dyn. Conf.*. Washington, D.C.

Kurelek, J. W., Lambert, A. R. & Yarusevych, S. 2016 Coherent Structures in the Transition Process of a Laminar Separation Bubble. *AIAA J.* **54** (8), 1–15.

Lissaman, P. B. S. 1983 Low-Reynolds-number airfoils. *Annu. Rev. Fluid Mech.* **15** (1), 223–239.

Marxen, O., Lang, M., Rist, U. & Wagner, S. 2003 A Combined Experimental/Numerical Study of Unsteady Phenomena in a Laminar Separation Bubble. *Flow, Turbul. Combust.* **71**, 133–146.

Matsubara, M. & Alfredsson, P. H. 2001 Disturbance growth in boundary layers subjected to free-stream turbulence. *J. Fluid Mech.* **430**, 149–168.

McAuliffe, B. R. & Yaras, M. I. 2010 Transition Mechanisms in Separation Bubbles Under Low- and Elevated-Freestream Turbulence. *J. Turbomach.* **132** (1), 011004.

Mueller, T. J. 1985 The influence of laminar separation and transition on low Reynolds number airfoil hysteresis. *J. Aircr.* **22** (9), 763–770.

Mueller, T. J., Conigliaro, P. & Jansen, B. J. 1983 The Influence of Free-Stream Disturbances on Low Reynolds Number Airfoil Experiments. *Exp. Fluids* **1**, 3–14.

Ol, M. V., McAuliffe, B. R., Hanff, E. S., Scholz, U., Kaehler, C., McCauliffe, B., Hanff, E. S., Scholz, U. & Kaehler, C. 2005 Comparison of Laminar Separation Bubble Measurements on a Low Reynolds Number Airfoil in Three Facilities. In *35th AIAA Fluid Dyn. Conf. Exhib.*. Toronto, Ontario.

Olson, D. A., Katz, A. W., Naguib, A. M., Koochesfahani, M. M., Rizzetta, D. P. & Visbal, M. R. 2013 On the challenges in experimental characterization of flow separation over airfoils at low Reynolds number. *Exp. Fluids* **54** (2), 1470.

O'Meara, M. M. & Mueller, T. J. 1987 Laminar separation bubble characteristics on an airfoil at low Reynolds numbers. *AIAA J.* **25** (8), 1033–1041.

Pröbsting, S. & Yarusevych, S. 2015 Laminar separation bubble development on an airfoil emitting tonal noise. *J. Fluid Mech.* **780**, 167–191.

Saric, W. S., Reed, H. L. & Kerschen, E. J. 2002 Boundary-Layer Receptivity to Freestream Disturbances. *Annu. Rev. Fluid Mech.* **34** (1), 291–319.

Tani, I. 1964 Low-speed flows involving bubble separations. *Prog. Aerosp. Sci.* **5**, 70–103.

Watmuff, J. H. 1999 Evolution of a wave packet into vortex loops in a laminar separation bubble. *J. Fluid Mech.* **397**, 119–169.

Welch, P. D. 1967 The Use of Fast Fourier Transform for the Estimation of Power Spectra: A Method Based on Time Averaging Over Short, Modified Periodograms. *IEEE Trans. audio Electroacoust.* **15** (2), 70–73.

Yarusevych, S. & Kotsonis, M. 2017*a* Effect of Local DBD Plasma Actuation on Transition in a Laminar Separation Bubble. *Flow, Turbul. Combust.* (98), 195–216.

Yarusevych, S. & Kotsonis, M. 2017*b* Steady and transient response of a laminar separation bubble to controlled disturbances. *J. Fluid Mech.* pp. 955–990.

Yarusevych, S., Sullivan, P. E. & Kawall, J. G. 2009 On vortex shedding from an airfoil in low-Reynolds-number flows. *J. Fluid Mech.* **632**, 245–271.

Zaki, T. A. 2013 From Streaks to Spots and on to Turbulence: Exploring the Dynamics of Boundary Layer Transition. *Flow, Turbul. Combust.* **91** (3), 451–473.